




Article

Multi-Stage ANN Model for Optimizing the Configuration of External Lightning Protection and Grounding Systems

Rohana Rohana ^{1,2}, Surya Hardi ³, Nasaruddin Nasaruddin ⁴ , Yuwaldi Away ^{4,*}  and Andri Novandri ⁴ 

¹ Doctoral Program, School of Engineering, Universitas Syiah Kuala, Banda Aceh 23111, Indonesia; rohana@umsu.ac.id

² Department of Electrical Engineering, Universitas Muhammadiyah Sumatera Utara, Medan 20238, Indonesia

³ Department of Electrical Engineering, Universitas Sumatera Utara, Medan 20155, Indonesia; surya.hardi@usu.ac.id

⁴ Department of Electrical and Computer Engineering, Universitas Syiah Kuala, Banda Aceh 23111, Indonesia; nasaruddin@usk.ac.id (N.N.); andrie.nov11@gmail.com (A.N.)

* Correspondence: yuwaldi@usk.ac.id

Abstract: This paper proposes an Artificial Neural Network (ANN) model using a Multi-Stage method to optimize the configuration of an External Lightning Protection System (ELPS) and grounding system. ELPS is a system designed to protect an area from damage caused by lightning strikes. Meanwhile, the grounding system functions to direct excess electric current from lightning strikes into the ground. This study identifies the optimal protection system configuration, reducing the need for excessive components. The ELPS configuration includes the number of protection pole units and the height of the protection poles. In contrast, the grounding system configuration consists of the number of electrode units and the length of the electrodes. This study focuses on the protection system configuration at a Photovoltaic Power Station, where the area is highly vulnerable to lightning strikes. Several aspects need to be considered in determining the appropriate configuration, such as average thunderstorm days per year, ELPS efficiency, total area of photovoltaic module, area to be protected, soil resistivity, electrode spacing factor, and the total required electrode resistance. The proposed multi-stage ANN model consists of three processing stages, each responsible for handling a portion of the overall system tasks. The first stage is responsible for determining the protection pole configuration. In the second stage, the Lightning Protection Level (LPL) classification is performed. Then, in the third stage, the process of determining the grounding configuration is handled. The analysis results show that the Multi-Stage ANN model can effectively determine the configuration with a low error rate: MAE of 0.265, RMSE of 0.314, and MPE of 9.533%. This model can also explain data variation well, as indicated by the high R^2 value of 0.961. The comparison results conducted with ATP/EMTP software show that the configuration produced by ANN results in fewer protection pole units but with greater height. Meanwhile, ANN produces a configuration with shorter electrode lengths but fewer units in the grounding system.

Keywords: ELPS; grounding; PV Station; multi-stage; ANN



Citation: Rohana, R.; Hardi, S.; Nasaruddin, N.; Away, Y.; Novandri, A. Multi-Stage ANN Model for Optimizing the Configuration of External Lightning Protection and Grounding Systems. *Energies* **2024**, *17*, 4673. <https://doi.org/10.3390/en17184673>

Academic Editors: Lin Zhu and Zhigang Wu

Received: 18 August 2024

Revised: 7 September 2024

Accepted: 14 September 2024

Published: 20 September 2024



Copyright: © 2024 by the authors. Licensee MDPI, Basel, Switzerland. This article is an open access article distributed under the terms and conditions of the Creative Commons Attribution (CC BY) license (<https://creativecommons.org/licenses/by/4.0/>).

1. Introduction

Lightning is a natural phenomenon that occurs when an electrical charge is discharged into the atmosphere [1]. This process happens due to a large electrical charge within a cloud. The charge then forms an electrical jump towards an area with a lower charge, whether within the cloud, between clouds, or to the ground [2]. A lightning strike to the ground risks causing structural damage to buildings and even fires. The electromagnetic field generated during a lightning strike can also induce electrical surges in electronic systems, causing damage and operational disruptions [3–5]. According to the study conducted in [6], transient voltage caused by lightning, whether direct or indirect, can lead to malfunctions or even damage to electrical equipment, thereby disrupting the transmission process.

An External Lightning Protection System (ELPS) is needed to prevent the fatal impacts of lightning strikes. ELPS is designed to protect and reduce the risk of lightning strikes [7]. This system functions to capture, conduct, and safely disperse lightning energy into the ground [8,9]. The main components of this system include the air termination, down conductor, and grounding system. The air termination captures lightning strikes in the air and then conducts the electric current through the down conductor to the grounding system. The electric current must be directed promptly to reduce the risk of electromagnetic induction [10]. The grounding system provides a safe path for the electric current to spread into the ground and can prevent backflow currents from damaging nearby electronic devices [11]. Several studies have examined the application of ELPS in various settings to protect buildings, such as industrial buildings [12], radar towers [13], and residential houses [14,15].

One of the systems highly vulnerable to lightning strikes is the Photovoltaic Power Station (PV Station). This is due to its location in large and open areas. Consequently, PV Stations have a high risk of direct lightning strikes [16]. A lightning strike can cause severe damage to the photovoltaic module, inverters, and other electronic components, potentially leading to financial losses and operational disruptions. Several studies have examined the application of ELPS to protect PV Stations, such as the paper [17], which discusses the impact of lightning strikes on PV systems and evaluates the necessary protection measures. Additionally, the paper [18] discusses the grounding system in ELPS by evaluating rod and plate electrode models. Furthermore, the paper [19] evaluates ELPS modelling using the rolling sphere method to protect PV Stations' electrical networks.

Lightning modelling is generally used for lightning prediction, ELPS design, and grounding systems [20]. Modelling for lightning prediction involves analyzing weather and climate conditions in a region by applying specific predictive algorithms, such as the Random Forest Classification algorithm discussed in [21]. The design of ELPS usually employs the rolling sphere method to determine the optimal protection radius, as discussed in [22]. Meanwhile, grounding system modelling involves using specific algorithms to determine electrode parameters, as explained in [23], which uses the Genetic Algorithm (GA). The goal is to achieve the lowest possible grounding resistance so that lightning current can be safely dispersed into the ground. The results of this study reveal that GA is a powerful optimization method for finding solutions to complex problems. However, GA has a slow optimization speed, so the model development process has yet to be fully generalized for various physical conditions of the electrodes. Several other studies have also examined lightning protection system modelling using specific methods. For instance, [24] discusses modelling using the Adaptive Neuro-Fuzzy Inference System (ANFIS) to predict lightning density in an area. This study produced the lowest RMSE during the training and testing, depending on the selected membership functions and system configuration. Additionally, the performance of ANFIS is highly dependent on the chosen parameters, which may require careful tuning to achieve optimal results. This reliance on algorithms and the selection of membership functions can be a weakness in ensuring the accuracy and generalization of the model across various conditions. Furthermore, [25] uses three meta-heuristic techniques: Particle Swarm Optimization (PSO), Genetic Algorithm Optimization (GAO), and Hybrid Particle Swarm Genetic Algorithm Optimization (HPSGAO). This study aims to design a grounding system by determining construction parameters that minimize costs and ensure optimization by ANSI/IEEE Std. 80–2000 safety standards. The study results indicate that HPSGAO, as the proposed method, yields lower total costs than GAO and PSO. However, this research has limitations regarding generalization to situations not covered in the study. In other words, the effectiveness of HPSGAO in reducing costs may only be fully applicable to some types of grounding systems or varying environmental conditions.

Additionally, other research uses Artificial Neural Network (ANN) algorithms as a modelling method. ANN is a computational system inspired by the human biological neural network and consists of layers of interconnected neurons. ANN can learn and

recognize complex patterns from data. Due to its ability to model non-linear relationships and handle unstructured data, ANN can be used as a predictive method, such as in ELPS modelling, to enhance effectiveness and efficiency against lightning strikes, as reviewed in [26]. This study examines the modelling of grounding resistance based on electrode types. The results show that the ANN model can estimate grounding resistance with an error rate of 5%. Furthermore, [27] discusses modelling to predict lightning locations. The study results indicate that the ANN model successfully identified lightning location coordinates with an average error of about 350 m. Then, in [28], a study was conducted on measuring the atmospheric electric field to study the cloud lightning discharge phenomenon. These measurement data were then processed using ANN to predict lightning activity. The study produced predictions with an accuracy of 88.2% and a precision rate of 92.2%. The paper [29] discusses the use of ANN as a model for estimating the risk of damage from lightning strikes. Additionally, ANN is used to identify factors that influence lightning strike risk, such as building location and environmental conditions. Risk assessment is conducted by classifying these factors based on photographs of an area surrounding the analyzed object. The study results indicate that using ANN for lightning risk assessment can significantly benefit ELPS designers. Several other literature studies related to ANN modelling in various lightning protection applications are also presented in Table 1. Based on the study, the method used is still a single-stage ANN approach. The single-stage ANN is the processing method, only performed in one stage without task division or processing. The single-stage approach has the drawback of needing help to handle data with significant variation, making it more challenging to update parts of the model without retraining the entire network. On the other hand, there is multi-stage ANN, a variant of ANN that involves several consecutive processing stages to enhance the model's accuracy and efficiency. In this method, each stage consists of one or more ANN layers responsible for handling specific tasks. The results of each stage are then used as input for the next stage, allowing the system to refine and improve prediction or classification results. Multi-stage ANN is beneficial when the problem is complex and requires comprehensive analysis that a single-stage ANN cannot achieve. As discussed in [30], the multi-stage ANN method can reduce processing time and provide superior predictions. Additionally, [31] shows that the results from applying multi-stage ANN achieve highly accurate statistical results that can be used for system design and optimization.

Table 1. Literature review of ANN applications in lightning and grounding.

Paper	Year	Application	Input Variables	%Accuracy	%Error
Kayabasi et al. [32]	2022	Classification Soil Type	Earth resistance	94.61	2.5
Chey et al. [33]	2021	Lightning Warning System	Pressure, temperature, relative humidity, precipitable water, and wind	-	-
Nielsen et al. [34]	2021	Estimating Lightning Damage	Peak current amplitude, rising time, and decaying time	-	-
Wang et al. [35]	2019	Lightning Warning System	Change rate of electromagnetic field, temperature, and humidity	93.9	-
Abdullah et al. [36]	2018	Lightning Forecasting	Air pressure, humidity, temperature, rainfalls, and wind	-	11.05
Neamt et al. [37]	2017	Measurement Grounding Resistance	Electrode length, soil layer thickness, and soil layer resistivity ratio	-	7.88

Table 1. Cont.

Paper	Year	Application	Input Variables	%Accuracy	%Error
Androvitsaneas et al. [38]	2014	Ground Resistance Forecasting	Rainfall of the day, rainfall during a week, rainfall during a month, and sinusoidal functions of one year	-	17.29
Omar et al. [39]	2013	Predict Severity of Lightning	Minimum humidity, maximum humidity, minimum temperature, maximum temperature, rainfall, week and month	70	14.67
Androvitsaneas et al. [40]	2012	Measurement Grounding Resistance	Soil resistivity for various distances, average soil resistivity, rainfall in the previous week, rainfall in the previous month, and rainfall during the day	-	-
Asimakopoulou et al. [41]	2011	Measurement Grounding Resistance	Soil resistivity for various distances, average rainfall in the previous week, rainfall during the day, and average resistance in the previous week	-	1.71
Johari et al. [42]	2009	Lightning Forecasting	Meteorological data, month indicator, and season indicator	-	-
Salam et al. [43]	2006	Measurement Grounding Resistance	Electrode length and month	92.5	-

This study proposes an ANN modeling to obtain the appropriate configuration for determining the required ELPS and grounding system to protect a PV Station area from lightning strikes. The determined configuration includes the number of protection pole units, the height of the protection poles, the number of electrode units, and the length of the electrodes. Unlike previous methods that often use a single-stage approach, this paper introduces a new ANN processing method that employs a multi-stage approach with three stages processed sequentially. In the first stage, processing is performed to determine the necessary protection pole configuration based on input such as average thunderstorm days per year, protection system efficiency, the total area of PV module, and the area to be protected. Next, in the second stage, processing is conducted to classify the Lightning Protection Level (LPL) based on the number and height of protection poles processed in the first stage. The result of the lightning protection level is then used to determine the resistance of the single-electrode in the third stage. Finally, in the third stage, the processing is conducted to determine the required grounding system configuration based on the input of soil resistivity, single-electrode resistance, electrode spacing factor, and total electrode resistance. This multi-stage approach can enhance lightning protection system design adaptability compared to the single-stage methodology. The dataset was collected from the Meteorology, Climatology, and Geophysics Agency and field measurements [44–48]. With these three processing stages, the ANN model can determine the ELPS and grounding system requirements, provide a design guide for lightning protection systems for PV Stations, and help reduce excessive components, thus making the protection system more efficient and economical. The main contributions of this paper are as follows:

- We propose developing an ANN model using a multi-stage method to determine the optimal and economical configuration for ELPS and grounding systems. The goal is to

address the complexity of data, which is often challenging to solve with single-stage methods.

- The proposed model consists of three stages processed sequentially. The first stage determines the ELPS configuration, the second classifies the LPL, and the third determines the grounding configuration. The goal is to overcome the shortcomings of the single-stage method, which often analyzes these elements separately, potentially leading to less integrated results. This model aims to create a more coherent solution by dividing the process into three stages, thereby enhancing the effectiveness and ensuring the utmost efficiency in determining ELPS and grounding configurations.
- We analyze the ANN model to determine performance levels through testing and validation using actual data. Then, we compare it with ATP/EMTP software to ensure that the proposed model configuration yields more optimal and economical results.

2. Materials and Methods

The model design in this work uses Python 3.10, a high-level programming language used for computation, data analysis, and visualization. The model's performance is then compared with the application output of the Alternative Transients Program/Electromagnetic Transients Program (ATP/EMTP). ATP/EMTP is simulation software used to model voltage surges caused by lightning strikes and grounding systems, aiding in the design of lightning protection and grounding systems.

2.1. External Lightning Protection System

The External Lightning Protection System (ELPS) is designed to protect areas or buildings from the impact of lightning strikes. This system generally consists of three main components: air termination, down conductor, and grounding system [49]. The air termination is the first part that receives the lightning strike, typically a metal rod installed at the highest point. In its implementation, the lightning protection system must consider several essential factors to achieve adequate protection, such as the number and height of the protection poles [50,51]. These factors will determine the coverage area to prevent damage from lightning strikes. The height of the protection pole affects the area that is protected. The higher the pole, the larger the radius of the protected area. Additionally, the higher the lightning rod, the smaller the protection angle. Both statements are demonstrated by the following equation [12],

$$r_p = h_p \tan \alpha^\circ \quad (1)$$

where, r_p is the protection radius, h_p is the height of the protection pole, and α° is the protection angle. The height of the protection pole is directly proportional to the protection radius, while the protection angle is inversely proportional to the height of the protection pole. This principle is based on the theory that lightning will strike the highest object in its vicinity, so installing a pole at the highest point will capture the lightning strike before it hits lower objects [52]. Additionally, the number of protection poles is crucial to creating an effective protection system. The number of poles installed will ensure that the protected area is well-covered. Distributing ELPS at various points can help form an effective protection network [53]. When determining the number and height of the poles, factors such as the area size, average thunderstorm days per year, and the efficiency of the lightning protection system must be carefully considered.

Average thunderstorm days per year is a metric that measures the average number of days in a year during which a location experiences thunderstorms. This parameter provides insight into the frequency of lightning activity in an area [54,55]. The value can vary significantly depending on geographical and climatic factors. Tropical regions such as Indonesia, Central Africa, and parts of South America tend to have high average thunderstorm days, potentially exceeding 100–200 days per year [56–58]. In contrast, regions with cold climates have meager average thunderstorm days, typically less than 10 days per year [59,60]. Average thunderstorm days data were collected from the lightning detection system owned by the Meteorology, Climatology, and Geophysics Agency.

The protection area size is a parameter that determines the extent of the area that ELPS can protect from lightning strikes. The protection area size can be calculated using the rolling sphere method, a geometric approach to determining the reach of lightning protection, as shown in Figure 1a. This method involves imagining a sphere rolling with a certain radius r . The value of this radius depends on the lightning protection level according to the International Electrotechnical Commission Standard (IEC), as listed in Table 2. As the sphere rolls over the ground surface, any part touched by the sphere is considered at risk of a lightning strike, while the parts not touched are protected, with a protection radius r_p . The height of the protection pole (h_p) is adjusted so that the sphere does not touch the area to be protected. Figure 1b illustrates the ELPS protecting a PV station with a total PV module area A_{pv} . By applying the rolling sphere method, the protection radius r_p is obtained, so the protected area is A_p . To calculate the protection radius r_p , the following equation is used,

$$r_p = \sqrt{h_p(2r - h_p)} \quad (2)$$

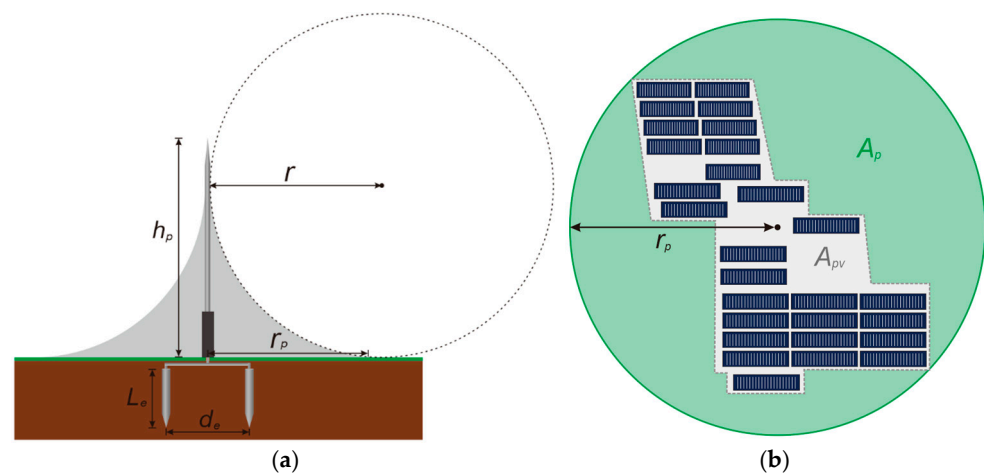


Figure 1. (a) External lightning protection and grounding system parameter, (b) The lightning protection area on the PV station.

Table 2. IEC standard lightning protection level.

Protection Level	Radius of Rolling Sphere (m)	Description
I	20	Highly critical structures
II	30	Important infrastructure
III	45	Standard commercial structures
IV	60	Low-risk structures

The efficiency of ELPS is the system's ability to protect an area from lightning strikes. This efficiency can be measured by how well the system can divert lightning current to the ground without causing damage to the protected area. To calculate the efficiency value, the following equation is used,

$$\eta_p = \frac{N_s}{N_{ts}} \quad (3)$$

where, N_s is the number of lightning strikes successfully captured by the ELPS and N_{ts} is the total number of lightning strikes that occur in the protected area. The number of lightning strikes is measured using the Lightning Detection System (LDS), which detects the electromagnetic waves generated by lightning strikes. This device is often installed along with the ELPS installation process.

In protecting an area from lightning strikes, classification is necessary to determine the level of protection the ELPS provides. The IEC standard provides guidelines on the

lightning protection levels that should be applied to various structures and environments. This standard includes different protection levels categorized based on lightning strikes' risk and potential impact [61]. There are four primary protection levels in IEC 62305-3 [62], as shown in Table 2. These protection levels assist in determining the design of the ELPS, including the height and number of poles, as well as the grounding system, to ensure effective and efficient protection tailored to the specific needs of each location [63].

ELPS is designed to handle electrical current surges reaching tens to hundreds of thousands of amperes. However, its specific capability depends on the specifications and classification of the ELPS used. To calculate the maximum current that the ELPS can protect, the following equation is used,

$$I_{max} = 0.75\sqrt{r} \quad (4)$$

where, I_{max} is the maximum lightning current and r is the radius of the rolling sphere.

2.2. Grounding System

The grounding system in a lightning protection system is an essential component that dissipates the electrical current from a lightning strike into the ground, thereby reducing the risk of damage to nearby objects [64]. This system consists of several components, including the electrode rod buried in the ground. The grounding resistance value must be calculated to measure how well a grounding system can conduct electrical current to the ground. The grounding resistance value can be calculated using the following equation [65,66],

$$R_s = \frac{\rho}{2\pi L_e} \left(\ln \left(\frac{4L_e}{d} \right) - 1 \right) \quad (5)$$

where, R_s is the resistance of a single electrode, ρ is the resistivity of the soil, L_e is the electrode length, and d is the electrode diameter. Meanwhile, to calculate the resistance value for multi-electrode, the following equation is used [67],

$$R_t = \frac{R_s}{N_e} \left(1 + \frac{N_e - 1}{2} k \right) \quad (6)$$

where, R_t is the total resistance, N_e is the number of electrodes, and k is the spacing factor, which can be calculated using the following equation,

$$k = \frac{1}{\ln \left(\frac{D}{d} \right)} \quad (7)$$

where, D is the distance between electrodes. To ensure optimal operation of the grounding system, it is necessary to determine the parameters of the number and length of electrodes required, as this will affect how effectively lightning currents can be dissipated into the ground [68,69]. Additionally, this can enhance economic value, as using suitable electrodes can reduce material and installation costs [70]. Several aspects must be considered to determine these parameters, such as the soil resistivity value in a specific area, electrode specifications, and the distance between electrodes.

The soil resistivity measures how much soil resists the flow of electric current. This value is expressed in ohm-meters (Ωm). Soil resistivity is influenced by various factors such as soil type, moisture content, and temperature [71]. Each soil type has varying resistivity values, as presented in Table 3. Low soil resistivity values indicate that the soil conducts electricity efficiently, allowing electric currents to be dissipated quickly into the ground. Conversely, high resistivity values suggest that the soil has more excellent resistance to electric current flow, which can reduce the effectiveness of the grounding system. The four-point method, also known as the Wenner method, is generally used to measure soil resistivity. This method involves inserting four metal electrodes into the ground at equal distances from each other in a straight line. A small electric current is then passed through the two outer electrodes, while the two inner electrodes measure the voltage generated

by the current. By knowing the magnitude of the current and the measured voltage, soil resistivity can be calculated using the following equation,

$$\rho = 2\pi D \frac{V}{I} \quad (8)$$

where, V is the voltage measured between the two electrodes and I is the current passed through the outer electrodes.

Table 3. Soil resistivity for grounding system.

Type of Soil	Resistivity Value (Ωm)
Moist Humus	30
Agricultural Soil	100
Sandy Clay	150
Clay	300
Dry Sand	400
Moist Sand	1000

Electrode specifications also affect the grounding system by selecting materials capable of optimal electrical conductivity. The distance between electrodes must also be considered to avoid mutual coupling effects [72]. Mutual coupling is a phenomenon where electrodes placed too close can electromagnetically influence one another. This can lead to interference or inefficiency in conducting electric current [73].

3. Multi-Stage ANN

Multi-stage ANN is a neural network architecture consisting of multiple processing stages, each of which handles a part of the overall process. Each stage in the ANN architecture consists of one or more hidden layers with several nodes that process data before passing the results to the next stage. This study uses a multi-stage ANN to determine the configuration of the ELPS and grounding system, optimizing the required component needs. The model design process is illustrated in the flowchart in Figure 2. This model uses vertical optimization to select the best structure at each stage based on statistical analysis and metric evaluation. The chosen structures are then combined into a single overall model. In the process, the output values at each node can be calculated using a linear combination based on the received input values [74]. These values are computed using the following equation,

$$z = \sum_{i=1}^n w_i \cdot x_i + b \quad (9)$$

where, x_i is the input value at node i , w_i is the weight value at input node i , b is the bias value, and z is the linear combination value at each node. Next, an activation function is applied to each output node in the network. Several commonly used activation functions, are Sigmoid, Tanh, and ReLU. Sigmoid is a non-linear function that transforms the output into a value between 0 and 1 using the following equation,

$$f(z) = \frac{1}{1 + e^{-z}} \quad (10)$$

where, e is the Euler's number, which is the base of the natural logarithm. Hyperbolic Tangent (Tanh) is also a non-linear function that transforms the output into a value between -1 and 1 using the following equation,

$$f(z) = \frac{e^z - e^{-z}}{e^z + e^{-z}} \quad (11)$$

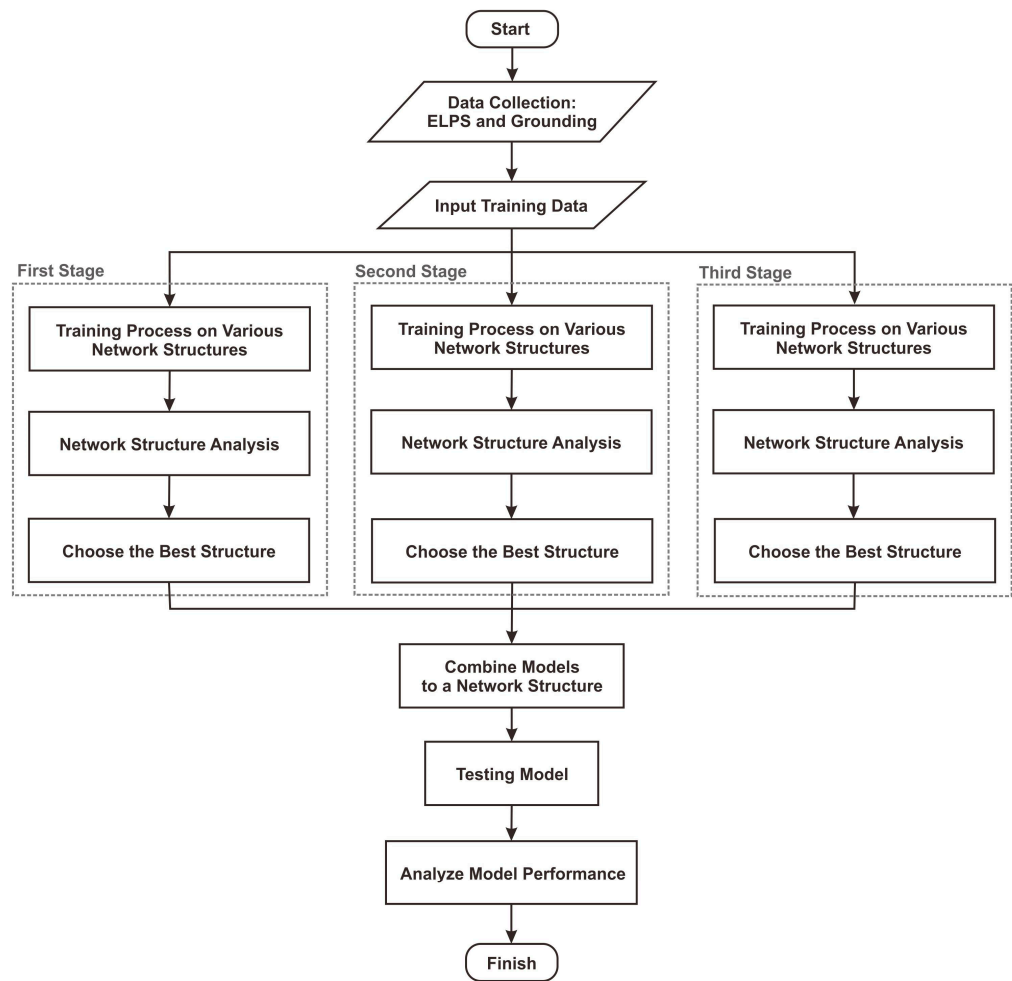


Figure 2. Flowchart for design of the model using multi-stage ANN.

Meanwhile, Rectified Linear Unit (ReLU) transforms the input into a value between 0 and infinity using the following equation,

$$f(z) = \max(0, z) \quad (12)$$

To design an ANN model, a learning process consisting of two main stages is required: Feedforward and Backpropagation [75]. Feedforward is the first stage in the ANN learning process. In this stage, input data are passed through the network from the input layer to the hidden layers until it reaches the output layer. Each node in the hidden layers receives input signals, applies an activation function, and then passes the results to the nodes in the next layer. The number of hidden layers depends on the data complexity and the model's ability to understand patterns from the training data [76,77]. The initial step of the Feedforward process is to compute the node values in hidden layer 1 using the following equation,

$$a^{(1)} = f\left(W^{(1)} \cdot x + b^{(1)}\right) \quad (13)$$

where, $a^{(1)}$, $W^{(1)}$, and $b^{(1)}$, respectively, represent the node values, weight matrix, and bias vector in the first hidden layer. The next step is to compute the node values in hidden layer n using the following equation,

$$a^{(n)} = f\left(W^{(n)} \cdot a^{(1)} + b^{(n)}\right) \quad (14)$$

where, $a^{(n)}$, $W^{(n)}$, and $b^{(n)}$, respectively, represent the node values, weight matrix, and bias vector in hidden layer n . Then, the node values in the output layer are calculated using the following equation,

$$a^{(n)} = f\left(W^{(n)} \cdot a^{(1)} + b^{(n)}\right) \quad (15)$$

where, y is the node value in the output layer. Next, the loss value is computed to measure the difference between the network output and the target value. The loss value is measured using Mean Squared Error (MSE), which calculates the average squared difference between the network output and target values. The MSE equation is as follows,

$$MSE = \frac{1}{n} \sum_{i=1}^n (y_i - \hat{y}_i)^2 \quad (16)$$

where, n is the number of datasets, y_i and \hat{y}_i represent the network output value and the target value for the i dataset, respectively.

Backpropagation is the second stage of training the model by adjusting weights and biases based on the loss value [78]. The Backpropagation process employs the gradient descent method to calculate the error gradient concerning each weight in the network and iteratively update weights and biases. This process minimizes errors and improves the model's prediction accuracy [79–81]. The gradient value of the loss concerning each weight is computed using the chain rule. If the loss function is L , then the gradient concerning weight w is as follows,

$$\frac{\partial L}{\partial w} = \frac{\partial L}{\partial \hat{y}} \cdot \frac{\partial \hat{y}}{\partial z} \cdot \frac{\partial z}{\partial w} \quad (17)$$

where, $\frac{\partial L}{\partial \hat{y}}$ is the derivative of the loss function concerning the predicted output \hat{y} , resulting in the function $2(y_i - \hat{y}_i)$. Meanwhile, $\frac{\partial \hat{y}}{\partial z}$ is the derivative of the activation function, and $\frac{\partial z}{\partial w}$ is the derivative of the linear combination z concerning the weight w . Next, the weight values are updated using the gradient and learning rate μ as follows,

$$w \leftarrow w - \mu \frac{\partial L}{\partial w} \quad (18)$$

Figure 3 shows the structure of the proposed multi-stage ANN model. This structure consists of three stages, each with varying hidden layers. Testing and analysis were conducted to determine each stage's network structure and suitable activation functions. In the first stage, the ANN receives inputs such as average thunderstorm days per year (T_d), total PV module area (A_{pv}), ELPS efficiency (η_p), and the size of the protected area (A_p). These input variables are processed to produce outputs: protection pole parameters, including the number of poles (N_p) and pole height (h_p). The study on the placement of protection poles at PV stations was previously discussed in a paper [19], where the optimal distance between the protection pole and the PV module is 12.31 m. The installation of the ELPS can affect the geometry of the PV modules, so if there is a change in position, recalculations are necessary to ensure that the PV system's performance is not compromised and lightning protection remains optimal. The installed protection pole is isolated, meaning it is not directly connected to the PV system, so lightning current surges will not affect other devices. The output from the first stage serves as input for the second stage, which produces the output of Lightning Protection Level (LPL) referring to the IEC standard listed in Table 2. There are several reasons why the input values of the number and height of protection poles are used in determining the LPL (Lightning Protection Level). The height of the pole is directly correlated with the protection radius it generates, making it a key parameter in determining the extent of the protected area. Additionally, the number of poles affects protection coverage over a larger area. Other factors typically considered in determining LPL, such as building structure characteristics, should be addressed in this study because the focus is on PV station protection, where the protected structure is

relatively low and differs from conventional buildings. Based on this protection level, the value of I_{max} is calculated, determining the value of ground resistance (R_s) based on the maximum lightning voltage in a region (V_{max}) and soil moisture. The relationship between ground resistance and soil moisture can be expressed by the following equation [82],

$$R_s = R_{s0} \cdot e^{-\alpha M} \tag{19}$$

where, R_{s0} is the ground resistance when soil moisture approaches 0, M is the soil moisture percentage, and α is an empirical constant dependent on specific soil conditions. The equation indicates that ground resistance is inversely proportional to soil moisture content. By incorporating the variables I_{max} and V_{max} , the following equation is obtained to determine the value of ground resistance,

$$R_s = \frac{V_{max}}{I_{max}} \cdot e^{-\alpha M} \tag{20}$$

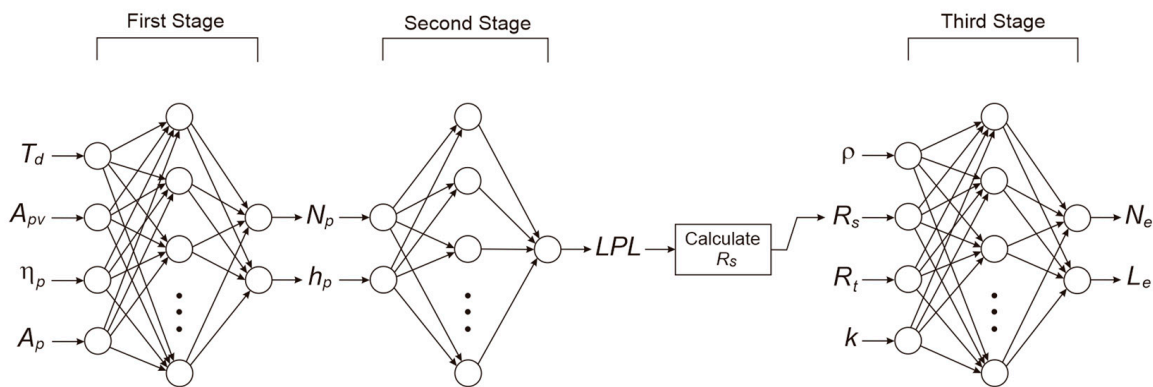


Figure 3. The structure of proposed multi-stage ANN model.

In the third stage, the ANN receives inputs such as R_s and additional variables like soil resistivity (ρ), desired total resistance (R_t), and the electrode spacing factor (k). The output from this stage provides grounding parameters, including the number of electrodes (N_e) and electrode length (L_e). These variables are selected based on the relationship between resistance variables and electrodes, as expressed in Equations (5) and (6). Subsequently, the three stages are trained to produce an optimal model. The sample input data used as the dataset are shown in Table 4.

Table 4. Sample input data.

T_d	A_{pv}	η_p	A_p	ρ	R_s	R_t	k
130	5369	0.70	6563	30	7.32	1.85	0.13
102	20164	0.77	21737	300	46.79	12.70	0.18
109	17984	0.73	22269	150	18.52	5.51	0.13
124	10438	0.70	13769	400	88.70	48.02	0.17
127	31533	0.89	34281	1000	139.74	75.15	0.15
114	25262	0.85	25850	100	12.48	3.17	0.13

4. Performance Analysis Method

The analysis is conducted to provide information on the performance results of the proposed model, including metric and statistical evaluations. One of the analysis methods is Mean Absolute Error (MAE), which is used to evaluate the model’s performance by calculating the average of the absolute differences between the predicted values and the

measured values. MAE provides an overview of the overall prediction error. The MAE equation is expressed as follows,

$$MAE = \frac{1}{n} \sum_{i=1}^n |y_i - \hat{y}_i| \quad (21)$$

where, n is the number of test data, y_i and \hat{y}_i are the actual and predicted values of the model for the i data, respectively. The lower the MAE value, the better the model's performance, indicating that the model's predictions are close to the actual values.

The following analysis is Root Mean Squared Error (RMSE), which measures the magnitude of the error between the predicted values by the model and the actual values. RMSE provides a measure that is more sensitive to significant errors than MAE. The equation is expressed as follows,

$$RMSE = \sqrt{\frac{1}{n} \sum_{i=1}^n (y_i - \hat{y}_i)^2} \quad (22)$$

Next is the analysis of Mean Percentage Error (MPE), which measures the deviation of the predictions from the actual values in percentage form. This result provides an overview of the model's accuracy on a relative scale. The equation is expressed as the average percentage error as follows,

$$MPE = \frac{1}{n} \sum_{i=1}^n \left(\frac{y_i - \hat{y}_i}{y_i} \right) \times 100\% \quad (23)$$

Next is the analysis of the Coefficient of Determination (R^2), a metric used to assess the performance of a regression model by measuring the proportion of data variability that the model can explain. The R^2 value ranges from 0 to 1, where 0 indicates that the model cannot explain the variability, while 1 indicates that the model can explain all the variability in the data. The R^2 value can be calculated using the following equation,

$$R^2 = 1 - \frac{\sum_{i=1}^n (y_i - \hat{y}_i)^2}{\sum_{i=1}^n (y_i - \bar{y})^2} \quad (24)$$

Then, there is the analysis of the Coefficient of Variation (CoV), a statistical measure used to evaluate the relative variability of data. CoV is generally used to assess data stability. A low CoV value indicates more stable data, while a high CoV value indicates more variable data. CoV is defined as the ratio of the standard deviation to the mean value, expressed as follows,

$$CoV = \frac{\sqrt{\frac{1}{n} \sum_{i=1}^n \left(y_i - \frac{1}{n} \sum_{i=1}^n y_i \right)^2}}{\frac{1}{n} \sum_{i=1}^n y_i} \quad (25)$$

The model's performance analysis is conducted by comparing the calculation results between the multi-stage ANN and ATP/EMTP. This comparison aims to evaluate the optimization achieved by the proposed model. The comparison process is carried out through computations based on a case study of lightning protection systems at a PV station on Sabang Island, Indonesia. The specifications of PV station are shown in Table 5. The protection parameters use a value of $\eta_p = 0.82$, $A_p = 19319.9 \text{ m}^2$, $R_t = 10 \text{ } \Omega$, and $k = 0.21$.

Table 5. Photovoltaic station specification.

Features	Value
Type	Polycrystalline
Total power	350 kWp
Open-circuit voltage	22.1 V
Short-circuit current	8.69 A
Total array	85 array
Module per array	25 module
Photovoltaic area	5577.11 m ²

5. Results and Discussion

In this section, the network evaluation is conducted to analyze the ANN structure at each stage and to evaluate the overall model performance. The network evaluation includes selecting the activation function and the number of hidden nodes for each stage. In this study, the model is trained using a dataset of 2000 data points, with 80% used for network training and 20% used for testing, with $\mu = 0.0002$. Meanwhile, no separate validation set was used, so the validation process was conducted internally using K-Fold Cross-Validation techniques to ensure the model was tested on various data subsets. This method utilizes the entire dataset for validation, rotating during k-fold iterations. The goal is to avoid overfitting and to build a model that can generalize well to test data [83,84]. The overall model output consists of protection pole parameters, such as the number and height of poles, and grounding parameters, such as the number and length of electrodes.

5.1. Model Analysis on First-Stage

Table 6 shows the statistical results from the network training process at the first stage based on various network structures. The statistical results indicate that the ReLU-32-14 structure performs best, with the lowest MAE, MSE, RMSE, and the highest R^2 , which are 0.27347, 0.15793, 0.76234, and 0.84207, respectively. Therefore, the structure at the first stage uses the ReLU activation function with 32 nodes in the first hidden layer and 14 nodes in the second hidden layer. The results also show that the ReLU function has better training speed, with an average more minor epoch than the sigmoid and tanh functions.

Table 6. The statistical results of training in the first stage.

Structure	Epoch	MAE	MSE	RMSE	R^2	CoV
Sigmoid-28-12	3627	0.28779	0.17384	0.79886	0.82616	0.7144
Sigmoid-32-14	3209	0.28818	0.17391	0.79949	0.82609	0.7093
Sigmoid-24-16-6	3467	0.2999	0.18393	0.81904	0.81607	0.7137
Sigmoid-28-20-8	4077	0.29227	0.17641	0.80573	0.82359	0.7091
Sigmoid-32-24-10	2739	0.29141	0.17672	0.80521	0.82328	0.7141
Sigmoid-36-28-12	2549	0.29001	0.17463	0.80227	0.82537	0.7161
Sigmoid-40-32-14	2642	0.28895	0.17328	0.7981	0.82672	0.7163
Tanh-28-12	924	0.29528	0.18204	0.81667	0.81796	0.7114
Tanh-32-14	1605	0.27829	0.16372	0.78258	0.83628	0.7107
Tanh-24-16-6	1103	0.31015	0.20011	0.85244	0.79989	0.709
Tanh-28-20-8	746	0.31349	0.20807	0.86399	0.79193	0.7097
Tanh-32-24-10	999	0.2915	0.1784	0.81468	0.8216	0.7176

Table 6. Cont.

Structure	Epoch	MAE	MSE	RMSE	R ²	CoV
Tanh-36-28-12	1289	0.28749	0.17366	0.80258	0.82634	0.7146
Tanh-40-32-14	1194	0.28809	0.17232	0.80405	0.82768	0.7116
ReLU-28-12	880	0.28554	0.16547	0.77629	0.83453	0.7024
ReLU-32-14	981	0.27347	0.15793	0.76234	0.84207	0.7089
ReLU-24-16-6	981	0.29414	0.17446	0.79813	0.82554	0.7023
ReLU-28-20-8	541	0.29722	0.17176	0.7832	0.82824	0.6955
ReLU-32-24-10	848	0.28119	0.15914	0.76355	0.84086	0.7015
ReLU-36-28-12	704	0.27561	0.15718	0.76236	0.84282	0.7038
ReLU-40-32-14	455	0.28172	0.16382	0.76865	0.83618	0.7119

Figure 4a presents the training results plot for the first stage for N_p and Figure 4b for h_p . These two graphs show that the data distribution shows a strong linear relationship between the measured data and the training results. However, some points are slightly outside the line, indicating some predictions deviating from the measurement data.

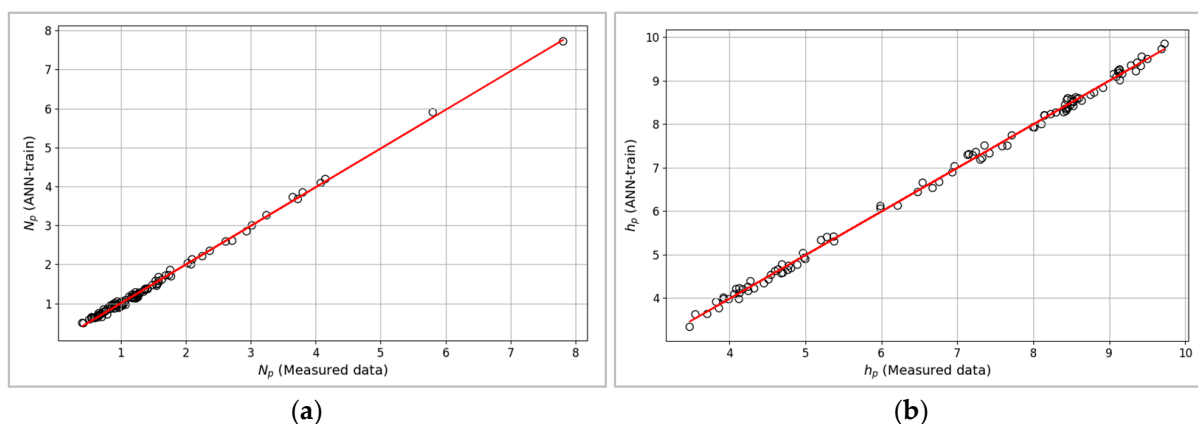


Figure 4. The training results at the first stage to determine (a) number of protection poles, (b) height of protection poles; The black circle was trained data and the red line was the reference line.

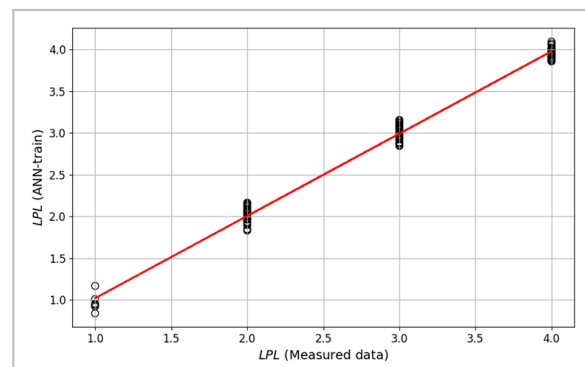
5.2. Model Analysis on Second-Stage

Table 7 presents the statistical results from the network training in the second stage. The statistical results show that the lowest MAE value in the ReLU-24-16-6 structure is 0.18643. Although this structure has the lowest MAE value, the ReLU-28-12 structure is considered the best based on a combination of several evaluation metrics, with the lowest MSE, RMSE, and the highest R^2 , which are 0.21911, 0.35199, and 0.78089, respectively. Therefore, the structure in the second stage uses the ReLU activation function with 28 nodes in the first hidden layer and 12 nodes in the second hidden layer.

Figure 5 presents the training results plot for the second stage. The graph shows the data points clustered into four groups, indicating the Lightning Protection Level (LPL) classification. This result shows that the model performs well in classifying LPL, with most data points closely matching the measured data.

Table 7. The statistical results of training in the second stage.

Structure	Epoch	MAE	MSE	RMSE	R ²	CoV
Sigmoid-28-12	2421	0.20685	0.22954	0.36027	0.77046	0.2277
Sigmoid-32-14	3284	0.20212	0.22936	0.36012	0.77064	0.2285
Sigmoid-24-16-6	3364	0.20448	0.2361	0.36538	0.7639	0.228
Sigmoid-28-20-8	2720	0.20255	0.23095	0.36137	0.76905	0.2279
Sigmoid-32-24-10	2395	0.204	0.23315	0.36309	0.76685	0.2284
Sigmoid-36-28-12	2728	0.20052	0.22942	0.36017	0.77058	0.2279
Sigmoid-40-32-14	2606	0.19656	0.23809	0.36691	0.76191	0.2303
Tanh-28-12	1271	0.20882	0.24898	0.37522	0.75102	0.2327
Tanh-32-14	1315	0.20497	0.24464	0.37193	0.75536	0.2324
Tanh-24-16-6	849	0.20804	0.26254	0.3853	0.73746	0.2349
Tanh-28-20-8	865	0.20588	0.25983	0.3833	0.74017	0.2343
Tanh-32-24-10	815	0.20615	0.25747	0.38156	0.74253	0.2349
Tanh-36-28-12	510	0.21938	0.27203	0.39219	0.72797	0.2329
Tanh-40-32-14	958	0.19947	0.24855	0.37489	0.75145	0.2352
ReLU-28-12	1466	0.19402	0.21911	0.35199	0.78089	0.2319
ReLU-32-14	600	0.20609	0.23131	0.36165	0.76869	0.2318
ReLU-24-16-6	889	0.18643	0.23065	0.36114	0.76935	0.2323
ReLU-28-20-8	833	0.20085	0.23216	0.36232	0.76784	0.226
ReLU-32-24-10	721	0.19423	0.23039	0.36093	0.76961	0.2285
ReLU-36-28-12	729	0.19426	0.23176	0.362	0.76824	0.2281
ReLU-40-32-14	976	0.19003	0.22811	0.35914	0.77189	0.2299

**Figure 5.** The training results in the second stage to determine the lightning protection level; The black circle was trained data and the red line was the reference line.

5.3. Model Analysis on Third-Stage

Table 8 presents the statistical results from the network training in the third stage. The statistical results indicate that the ReLU-40-32-14 structure performs the best compared to other structures. This structure shows the lowest MAE, MSE, and RMSE values with the highest R², which are 0.12575, 0.02897, 0.40608, and 0.97103, respectively. Therefore, the structure in the third stage uses the ReLU activation function with 40 nodes in the first hidden layer, 32 nodes in the second hidden layer, and 14 nodes in the third hidden layer.

Table 8. The statistical results of training in the third stage.

Structure	Epoch	MAE	MSE	RMSE	R ²	CoV
Sigmoid-28-12	298	0.53467	0.41994	1.40328	0.58006	0.4348
Sigmoid-32-14	255	0.55522	0.45159	1.45114	0.54841	0.4227
Sigmoid-24-16-6	1314	0.34843	0.20372	0.97379	0.79628	0.4696
Sigmoid-28-20-8	744	0.37457	0.231	1.04294	0.769	0.4695
Sigmoid-32-24-10	1617	0.29247	0.15022	0.84192	0.84978	0.4778
Sigmoid-36-28-12	1616	0.28628	0.14746	0.84039	0.85254	0.4851
Sigmoid-40-32-14	1296	0.29628	0.15765	0.86225	0.84235	0.477
Tanh-28-12	355	0.21156	0.08445	0.66494	0.91555	0.5131
Tanh-32-14	399	0.20741	0.07895	0.62698	0.92105	0.5157
Tanh-24-16-6	736	0.19848	0.06975	0.62507	0.93025	0.529
Tanh-28-20-8	478	0.20748	0.07258	0.60554	0.92742	0.5303
Tanh-32-24-10	494	0.18447	0.06115	0.56061	0.93885	0.5268
Tanh-36-28-12	499	0.16807	0.0471	0.50839	0.9529	0.5275
Tanh-40-32-14	819	0.14139	0.03774	0.45421	0.96226	0.5277
ReLU-28-12	1249	0.13041	0.0326	0.40923	0.9674	0.5405
ReLU-32-14	954	0.12882	0.03124	0.41689	0.96876	0.5311
ReLU-24-16-6	430	0.19138	0.06725	0.57882	0.93275	0.5078
ReLU-28-20-8	315	0.21519	0.07475	0.61026	0.92525	0.5068
ReLU-32-24-10	509	0.14943	0.03696	0.44417	0.96304	0.5184
ReLU-36-28-12	721	0.14807	0.03561	0.44858	0.96439	0.52
ReLU-40-32-14	695	0.12575	0.02897	0.40608	0.97103	0.5215

Figure 6a for N_e and Figure 6b for L_e present the training results plot for the third stage. Both graphs show that the data are well distributed around the reference line, indicating that the trained model performs very well in predicting the values of N_e and L_e .

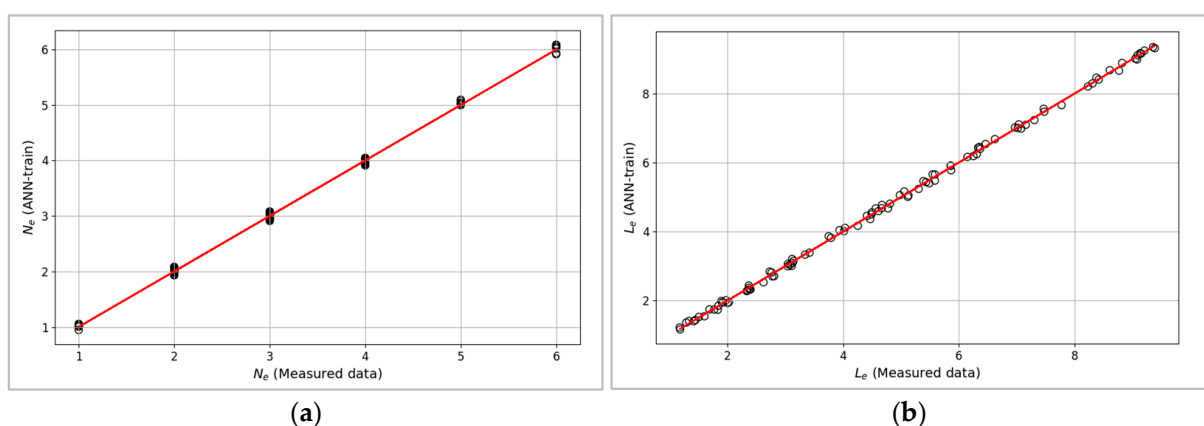


Figure 6. The training results at the third stage to determine (a) number of electrode grounding, (b) length of electrode grounding; The black circle was trained data and the red line was the reference line.

5.4. Model Performance on Predicting ELPS and Grounding Configurations

Figure 7a compares N_p values between the measured data and the model's predicted data. "Measurement data" refers to data obtained through direct field observations by studying various variables. In other words, these data are actual data used as a reference to evaluate the performance of the ANN model. Based on the graph, it is evident that the ANN predictions follow the trend of the measured data well, although there are some errors at higher values. The ANN predictions are pretty accurate for data with $N_p < 5$, with a distribution that almost follows the measured data. However, for values of $N_p > 6$, it is seen that the ANN predictions tend to deviate from the measured data. Meanwhile, Figure 7b shows the comparison results for h_p values. Based on this graph, the model demonstrates pretty good performance in following the trend of the measured data. However, as with Figure 7a, some deviations at significantly higher h_p values indicate more significant data variability at specific values. Then, Figure 8a shows the comparison results for N_e values. Based on the graph, the ANN prediction results exhibit more significant variation around the measured data. Although the ANN can capture the pattern, the predicted data have more variation. Next, Figure 8b shows the comparison results for L_e values. Based on the graph, the prediction results also show a similar linear trend, with minor deviations throughout the plot. Despite some slight deviations, the model predicts reasonably well.

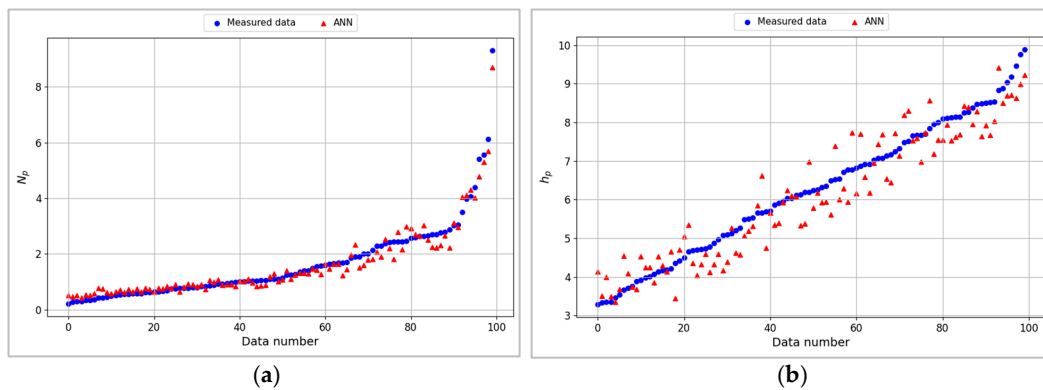


Figure 7. The testing result to determine the protection pole parameters (a) number of protection poles, (b) height of protection poles.

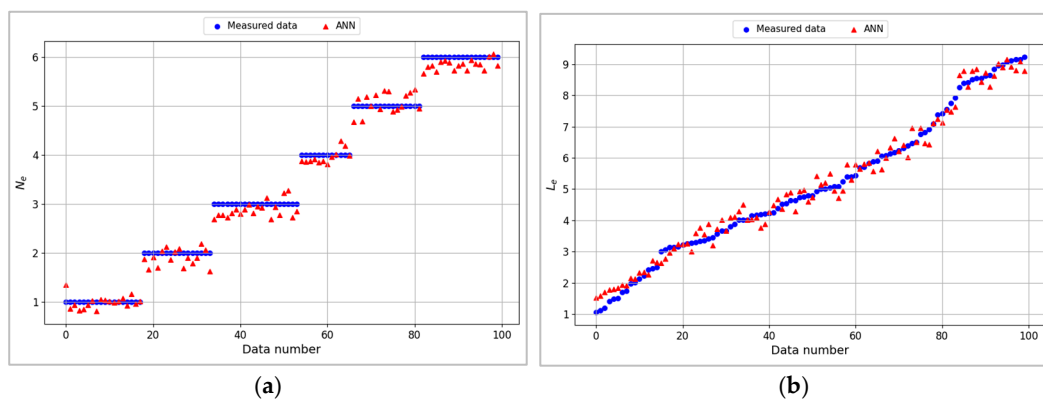


Figure 8. The testing result to determine the grounding parameters (a) number of electrodes, (b) length of electrodes.

Based on these results, the ANN model shows more significant prediction variability than the measured data. This is due to overfitting, a condition where the model fits the training data too closely, resulting in excellent performance on the training data but poor generalization to new data. Nevertheless, the model achieves low error values based on the test analysis results in Table 9. The ANN model performs well for the N_p parameter with relatively low MAE and RMSE. The R^2 value of 0.968 indicates that the model can

explain 96.8% of the variability in the data, though an MPE of 18.03% shows a relatively large error. A CoV value of 0.152 indicates fairly low variability, suggesting that the data are relatively consistent and not spread far from the mean value. The ANN model also performs well for the h_p parameter, although it has relatively higher MAE and RMSE than N_p . The R^2 value of 0.9 indicates that the model can explain 90% of the variability in the data. An MPE of 7.96% and CoV of 0.084 suggest that the relative error and prediction variability are relatively low. The N_e parameter shows the best performance with very low MAE and RMSE. The R^2 value of 0.989 indicates that the model almost entirely explains the variability in the data. An MPE of 5.65% and CoV of 0.05 signify accurate predictions with low relative error and variability. The ANN model also performs very well for the L_e parameter, with low MAE and RMSE. The R^2 value of 0.985 indicates that the model can explain 98.5% of the variability in the data. The MPE of 6.49% and CoV of 0.053 suggest that the model has low relative error and variability.

Table 9. The analytical result of the multi-stage ANN model to determine external lightning protection and grounding system.

Parameter	MAE	RMSE	MPE	R^2	CoV
N_p	0.199	0.252	18.03%	0.968	0.152
h_p	0.472	0.545	7.96%	0.9	0.084
N_e	0.154	0.185	5.65%	0.989	0.05
L_e	0.233	0.272	6.49%	0.985	0.053

5.5. Comparison Results with Multi-Stage ANN Model and ATP/EMTP

Table 10 compares the ELPS and grounding parameter requirements using the ANN model and ATP/EMTP software. Figure 9 shows the ELPS diagram from the ATP/EMTP software. The diagram consists of several parts, from the top with the air termination to the grounding system. The grounding system comprises several parallel circuits representing electrodes embedded in the ground. The number of electrodes required depends on various parameters, including lightning parameters and soil characteristics.

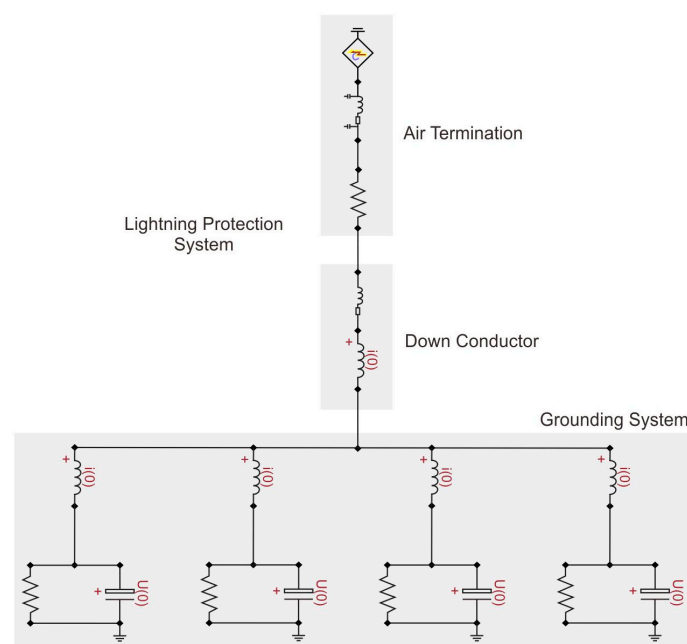


Figure 9. Circuit diagram of lightning protection and grounding system on ATP/EMTP.

Table 10. The comparison of multi-stage ANN and ATP/EMTP calculation results.

T_d (Days/Year)	ρ (Ωm)	Multi-Stage ANN				ATP/EMTP			
		N_p (unit)	h_p (m)	N_e (unit)	L_e (m)	N_p (Unit)	h_p (m)	N_e (unit)	L_e (m)
147	732	2	3.4	2	8.1	1	9.2	2	8.8
197	546	2	3.1	3	4.8	1	7.9	4	8.9
176	362	2	3.1	2	1.4	1	8.0	3	1.2
144	935	2	3.6	2	10.4	2	3.8	4	5.5
122	567	1	5.5	2	5.2	1	7.6	2	7.9
194	712	2	3.1	1	8.0	1	6.7	3	2.6
175	949	2	3.1	1	10.6	1	6.2	2	9.6
159	554	2	3.3	3	5.0	2	5.3	5	7.0
118	456	1	6.0	2	2.7	1	9.5	4	2.2
175	391	2	3.1	6	1.7	2	5.0	4	8.3
105	686	1	7.4	1	7.3	2	3.4	2	2.9
200	746	2	3.1	2	8.2	1	8.5	3	7.2
129	930	1	4.9	1	10.4	2	3.9	2	5.7
185	928	2	3.1	1	10.4	1	6.2	2	5.4
199	473	2	3.1	2	3.0	1	6.6	1	5.5
167	557	2	3.2	3	5.0	2	3.4	2	8.7
112	883	1	6.7	2	9.8	2	5.0	4	6.0
117	594	1	6.1	3	5.5	1	9.1	6	2.8
111	546	1	6.9	4	4.8	1	7.4	5	3.8
147	732	2	3.4	2	8.1	1	9.2	2	8.8

The results indicate that each method has a different configuration for specific input parameters. In some cases, the ANN tends to require fewer protection pole units but with greater height, whereas ATP/EMTP shows a more significant number of protection pole units with lower height. For example, with an average thunderstorm days per year of 105 days/year and soil resistivity of 686 Ωm , the ANN requires only one protection pole unit with a height of 7.4 m, while ATP/EMTP requires two units with a height of 3.4 m. Based on the height of the protection pole, the protection radius can be calculated with the lightning protection level at Level 1, corresponding to a rolling sphere radius of 20 m. The calculations yield a protection radius of 11.1 m in ATP/EMTP and 15.5 m in the multi-stage ANN. For clarity, these results are visualized in Figure 10. Meanwhile, Figure 11 compares protection areas based on the height and number of poles. In ATP/EMTP, the protection pole height is lower, resulting in a smaller protection area. Therefore, two unit poles are required to cover the entire region. In contrast, the pole height is more significant in the multi-stage ANN, leading to a more extensive protection area. This is why only one unit protection pole is needed. Similarly, for the grounding system, the ANN needs only one electrode unit with a length of 7.3 m, while ATP/EMTP needs two units with a length of 2.9 m. In other cases, the ANN tends to have more pole units with lower height compared to ATP/EMTP, such as in conditions with an average thunderstorm days per year of 176 days/year and soil resistivity of 362 Ωm , where the ANN requires two protection poles with a height of 3.1 m. Conversely, ATP/EMTP requires only one pole with a height of 8 m. Further results show that in some cases with higher soil resistivity, such as 935 Ωm and average thunderstorm days per year of 144 days/year, the ANN produces a configuration with two protection poles, each 3.6 m tall. In contrast, ATP/EMTP shows

a similar number of poles but with a slightly lower height, 3.8 m. However, differences appear in the grounding electrode requirements, where the ANN needs two electrodes with a length of 10.4 m, while ATP/EMTP requires four electrodes with a shorter length of 5.5 m.

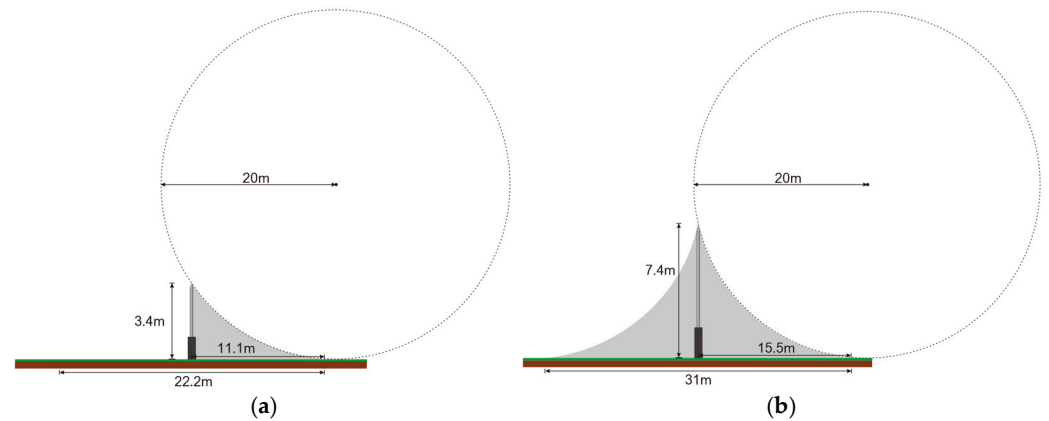


Figure 10. The comparison of protection radius based on pole height using different approaches (a) ATP/EMTP, (b) Multi-stage ANN.

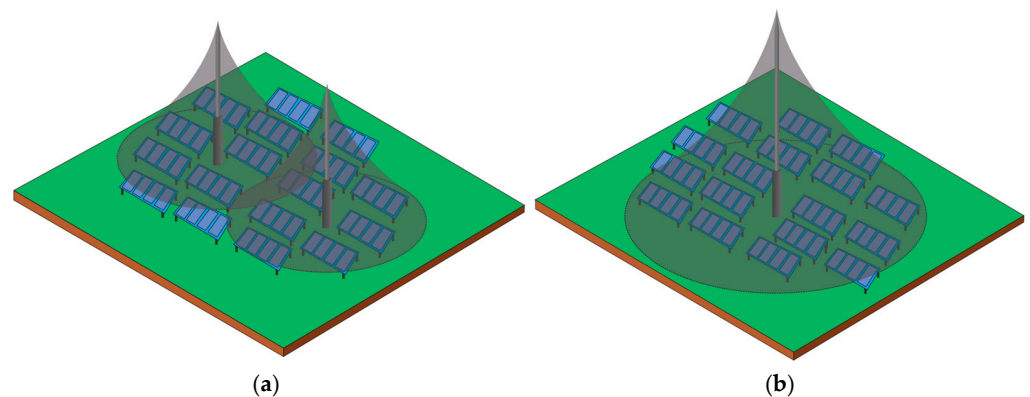


Figure 11. The comparison of protection areas based on pole height using different approaches (a) ATP/EMTP, (b) Multi-stage ANN.

This analysis indicates that the ANN model and ATP/EMTP provide varying configurations regarding the number and height of protection poles and the number and length of grounding electrodes, depending on specific environmental conditions such as soil resistivity and average thunderstorm days per year. The optimization comparison shows that the ANN tends to simplify the configuration with fewer units but emphasizes physical characteristics, such as taller poles. At the same time, ATP/EMTP offers a more traditional solution with a higher number of units but more moderate sizes.

6. Conclusions

The results of this study indicate that the multi-stage ANN model, as a predictive algorithm, can provide excellent results in predicting protection pole parameters and grounding parameters. The model consists of three stages: the first for predicting protection pole parameters, the second for classifying protection levels, and the third for predicting grounding parameters. In the first stage, the most optimal network structure uses two hidden layers with 32 and 14 nodes, respectively. The most optimal network structure in the second stage uses two hidden layers with 28 and 12 nodes, respectively. In the third stage, the most optimal network structure uses three hidden layers with 40, 32, and 14 nodes, respectively. Experimental results show that the ReLU function is the most suitable for all stages of the ANN. The training process statistics for protection pole parameters yield

MAE, RMSE, R^2 , and CoV values of 0.273, 0.762, 0.842, and 0.709, respectively, while the testing process values are 0.336, 0.399, 0.934, and 0.118, respectively. Meanwhile, for grounding parameters, the training process statistics yield MAE, RMSE, R^2 , and CoV values of 0.126, 0.406, 0.971, and 0.522, respectively, while the testing process values are 0.194, 0.229, 0.987, and 0.052, respectively. These results indicate that the ANN model can accurately predict protection pole and grounding parameters. Furthermore, the comparison between the multi-stage ANN model and ATP/EMTP software shows that the ANN tends to produce configurations with fewer protection pole units but greater height than ATP/EMTP. Additionally, the ANN often results in shorter electrode lengths and fewer units in the grounding system.

However, this study has several limitations, including the complexity of the model, which leads to overfitting. The proposed ANN model shows good performance during training but experiences overfitting during testing, resulting in reduced performance on new data. Additionally, this study does not consider all environmental factors that can affect the performance of the lightning protection system, such as soil conditions, humidity, and weather variations. Consequently, the study's results are limited to specific conditions and may not fully apply to different situations. Further research is needed to account for various environmental factors to improve the model's generalization and ensure its effectiveness in diverse environmental conditions. This study has successfully examined the vertical selection of network structures at each stage. Although the best structure from each stage was selected, there is still a possibility that combinations of not-best structures could yield better performance. However, an in-depth study on this has yet to be conducted. To address this, future research could focus on horizontal optimization by testing combinations of not-best structures to explore whether these combinations can enhance the model's overall performance.

Author Contributions: Conceptualization, R.R., S.H., N.N., Y.A. and A.N.; methodology, R.R., S.H., N.N., Y.A. and A.N.; software, R.R. and A.N.; validation, R.R., Y.A. and A.N.; formal analysis, A.N.; investigation, R.R., Y.A. and A.N.; resources, R.R., S.H., N.N. and Y.A.; data curation, R.R., S.H., N.N. and Y.A.; writing—original draft preparation, A.N.; writing—review and editing, R.R., Y.A. and A.N.; visualization, A.N.; supervision, R.R.; project administration, R.R.; funding acquisition, R.R. All authors have read and agreed to the published version of the manuscript.

Funding: This research received no external funding.

Data Availability Statement: Data is contained within the article.

Conflicts of Interest: The authors declare no conflicts of interest.

References

1. Fontanarosa, P.B. Electrical Shock and Lightning Strike. *Ann. Emerg. Med.* **1993**, *22*, 378–387. [[CrossRef](#)] [[PubMed](#)]
2. Chiradeja, P.; Ngaopitakkul, A. Identify Direct Lightning Strike Location Based on Discrete Wavelet Transform for 115-KV Transmission System. *IEEE Access* **2022**, *10*, 80609–80622. [[CrossRef](#)]
3. Maslowski, G. Measurements and Modeling of Electromagnetic Disturbances in the Lightning Protection System of the Residential Building. *Prz. Elektrotechniczny* **2016**, *1*, 66–69. [[CrossRef](#)]
4. Asif, M.; Lee, H.-Y.; Khan, U.A.; Park, K.-H.; Lee, B.W. Analysis of Transient Behavior of Mixed High Voltage DC Transmission Line Under Lightning Strikes. *IEEE Access* **2019**, *7*, 7194–7205. [[CrossRef](#)]
5. Huo, H.; Wang, D.; Chen, H.; Zhao, C.; Cheng, Q. Considering the Methods of Lightning Protection and Early Warning for Power Transmission Lines Based on Lightning Data Analysis. *IEEE Access* **2024**, *12*, 54168–54181. [[CrossRef](#)]
6. Ianoz, M. Lightning Electromagnetic Effects: Do We Know Everything? *Radio Sci.* **2003**, *304*, 17–33.
7. Gomes, A.; Gomes, C.; Kadir, M.Z.K.A.; Izadi, M.; Rock, M. Evaluation of Lightning Protection Systems Proposed for Small Structures by Electromagnetic Simulation. In Proceedings of the 33rd International Conference on Lightning Protection (ICLP), Estoril, Portugal, 25–30 September 2016; pp. 1–5.
8. Wang, Y.; Zhang, X.; Tao, S. Modeling of Lightning Transients in Photovoltaic Bracket Systems. *IEEE Access* **2019**, *7*, 12262–12271. [[CrossRef](#)]
9. Srinivasan, V.; Fernando, M.; Kumara, S.; Selvaraj, T.; Cooray, V. Modeling and Assessment of Lightning Hazards to Humans in Heritage Monuments in India and Sri Lanka. *IEEE Access* **2020**, *8*, 228032–228048. [[CrossRef](#)]

10. Sobolewski, K. Analysis of Lightning Current Distribution in the Lightning Protection System (LPS) with Using Numerical Simulations. *Prz. Elektrotechniczny* **2013**, *89*, 264–266.
11. Santoro, F.; Anifantis, A.S.; Ruggiero, G.; Zavadskiy, V.; Pascuzzi, S. Lightning Protection Systems Suitable for Stables: A Case Study. *Agriculture* **2019**, *9*, 72. [[CrossRef](#)]
12. Negara, I.M.Y.; Fahmi, D.; Asfani, D.A.; Hernanda, I.S.; Pratama, R.B.; Ksatria, A.B. Investigation and Improvement of Standard External Lightning Protection System: Industrial Case Study. *Energies* **2021**, *14*, 4118. [[CrossRef](#)]
13. Supartono, E.; Haryono, T. Suharyanto Application of Cone Protection and Rolling Sphere Methods in External Lightning Protection Analysis on 214 Radar Tower. *Int. J. Adv. Eng. Technol.* **2015**, *8*, 475–481.
14. Wang, P.; Li, L.; Rakov, V.A. Calculation of Current Distribution in the Lightning Protective System of a Residential House. *IEEE Trans. Magn.* **2014**, *50*, 225–228. [[CrossRef](#)]
15. Maslowski, G. Experimental Investigation and Numerical Modeling of Surge Currents in Lightning Protection System of a Small Residential Structure. *J. Light. Res.* **2012**, *4*, 18–26. [[CrossRef](#)]
16. Nicora, M.; Tucci, M.; Barmada, S.; Brignone, M.; Procopio, R. Lightning Location and Peak Current Estimation From Lightning-Induced Voltages on Transmission Lines With a Machine Learning Approach. *IEEE Trans. Electromagn. Compat.* **2024**, *66*, 890–899. [[CrossRef](#)]
17. Christodoulou, C.A.; Ekonomou, L.; Gonos, I.F.; Papanikolaou, N.P. Lightning Protection of PV Systems. *Energy Syst.* **2016**, *7*, 469–482. [[CrossRef](#)]
18. Rohana, R.; Hardi, S.; Nasaruddin, N.; Away, Y. Comparative Analysis of The Effective Grounding System on External LPS Modeling in PV Fields. In Proceedings of the 7th International Conference on Electrical, Telecommunication and Computer Engineering (ELTICOM), Medan, Indonesia, 13–14 December 2023; pp. 122–127.
19. Rohana, R.; Hardi, S.; Nasaruddin, N.; Away, Y. External Lightning Protection System Modeling on Photovoltaic Using ATP Draw. In Proceedings of the 10th International Conference on Electrical Engineering, Computer Science and Informatics (EECSI), Palembang, Indonesia, 20–21 September 2023; pp. 84–89.
20. RAHEEM, B.; Ogbuju, E.; Oladipo, F. Development of a Lightning Prediction Model Using Machine Learning Algorithm: Survey. *J. Appl. Artif. Intell.* **2023**, *4*, 45–56. [[CrossRef](#)]
21. Blouin, K.D.; Flannigan, M.D.; Wang, X.; Kochtubajda, B. Ensemble Lightning Prediction Models for the Province of Alberta, Canada. *Int. J. Wildl. Fire* **2016**, *25*, 421. [[CrossRef](#)]
22. Martínez, J.M.; Angarita, E.M.N.; Alvarez, J.R.N.; Crespo, M.H.; Pertuz, P.J.F. Lightning Rod System: Mathematical Analysis Using the Rolling Sphere Method. *Int. J. Power Electron. Drive Syst.* **2022**, *13*, 237–246. [[CrossRef](#)]
23. Mishra, A.K.; Nagaoka, N.; Ametani, A. A Genetic Algorithm Approach for Modeling a Grounding Electrode. *IEEE Trans. Power Energy* **2005**, *125*, 816–821. [[CrossRef](#)]
24. Said, S.M.; Nappu, M.B.; Asri, A.; Utomo, B.T. Prediction of Lightning Density Value Tower Based on Adaptive Neuro-Fuzzy Inference System. *Arch. Electr. Eng.* **2024**, *70*, 499–511. [[CrossRef](#)]
25. Alik, B.; Teguar, M.; Mekhaldi, A. Minimization of Grounding System Cost Using PSO, GAO, and HPSGAO Techniques. *IEEE Trans. Power Deliv.* **2015**, *30*, 2561–2569. [[CrossRef](#)]
26. Bhosale, M.; Karandikar, P.B.; Karkaria, V.; Kulkarni, N.R. A Novel Approach for Grounding Resistance Estimation. *Indones. J. Electr. Eng. Comput. Sci.* **2022**, *27*, 583. [[CrossRef](#)]
27. Mehrazamir, K.; Abdul-Malek, Z.; Nabipour Afrouzi, H.; Vahabi Mashak, S.; Wooi, C.; Zarei, R. Artificial Neural Network Application in An Implemented Lightning Locating System. *J. Atmos. Sol.-Terr. Phys.* **2020**, *210*, 105437. [[CrossRef](#)]
28. Bao, R.; Zhang, Y.; Ma, B.J.; Zhang, Z.; He, Z. An Artificial Neural Network for Lightning Prediction Based on Atmospheric Electric Field Observations. *Remote Sens.* **2022**, *14*, 4131. [[CrossRef](#)]
29. Sobieska, E. Investigation of the Possibility of Using Artificial Neural Networks in the Process of Assessing the Threat of Lightning. *Przegląd Elektrotechniczny* **2023**, *1*, 213–216. [[CrossRef](#)]
30. Bakhary, N.; Hao, H.; Deeks, A.J. Substructuring Technique for Damage Detection Using Statistical Multi-Stage Artificial Neural Network. *Adv. Struct. Eng.* **2010**, *13*, 619–639. [[CrossRef](#)]
31. Senturk Acar, M. Multi-Stage Artificial Neural Network Structure-Based Optimization of Geothermal Energy Powered Kalina Cycle. *J. Therm. Anal. Calorim.* **2021**, *145*, 829–849. [[CrossRef](#)]
32. Kayabasi, A.; Yildiz, B.; Balci, S. An Artificial Neural Network Model Based on Experimental Measurements for Estimating the Grounding Resistance. *Adv. Artif. Intell. Res.* **2022**, *2*, 29–37. [[CrossRef](#)]
33. Chey, C.O.; Sriv, T. Early Warning and Protection Systems for Lightning Strike in Cambodia Based on Meteorological Data and Human Action. 2021. Available online: https://www.researchgate.net/profile/Tharith_Sriv/publication/335101481_Early_Warning_and_Protection_Systems_for_Lightning_Strike_in_Cambodia_Based_on_Meteorological_Data_and_Human_Action/links/5ff3f0c492851c13feeb57b9/Early-Warning-and-Protection-Systems-for-Lightning-Strike-in-Cambodia-Based-on-Meteorological-Data-and-Human-Action.pdf (accessed on 4 May 2024).
34. Niealsen, D.; Lott, T.; Dutta, S.; Lee, J. Artificial Neural Network (ANN)-Based Predictive Tool for Estimating Lightning Damage in Composites. In Proceedings of the American Society for Composites (ASC) Technical Conference, College Station, TX, USA, 19–23 September 2021; Volume 2, pp. 1019–1034.

35. Wang, G.; Kim, W.-H.; Kil, G.-S.; Park, D.-W.; Kim, S.-W. An Intelligent Lightning Warning System Based on Electromagnetic Field and Neural Network. *Energies* **2019**, *12*, 1275. [[CrossRef](#)]
36. Abdullah, N.H.; Adnan, R.; Samad, A.M.; Ahmat Ruslan, F. Lightning Forecasting Modelling Using Artificial Neural Network (ANN): Case Study Sultan Abdul Aziz Shah Airport or Skypark Subang. In Proceedings of the IEEE Conference on Systems, Process and Control (ICSPC), Melaka, Malaysia, 14–15 December 2018; pp. 1–4.
37. Neamt, L.; Matei, O.; Chiver, O. Finite Element Method Combined with Neural Networks for Power System Grounding Investigation. *Int. J. Adv. Comput. Sci. Appl.* **2017**, *8*, 187–192. [[CrossRef](#)]
38. Androvitsaneas, V.P.; Tsekouras, G.J.; Gonos, I.F.; Stathopoulos, I.A. Design of an Artificial Neural Network for Ground Resistance Forecasting. In Proceedings of the 9th Mediterranean Conference on Power Generation, Transmission, Distribution and Energy Conversion, Athens, Greece, 2–5 November 2014.
39. Azhar Omar, M.; Khair Hassan, M.; Che Soh, A.; Kadir, M.Z.A.A. Lightning Severity Classification Utilizing the Meteorological Parameters: A Neural Network Approach. In Proceedings of the International Conference on Control System, Computing and Engineering, Penang, Malaysia, 29 November–3 December 2013; pp. 111–116.
40. Androvitsaneas, V.P.; Asimakopoulou, F.E.; Gonos, I.F.; Stathopoulos, I.A. Estimation of Ground Enhancing Compound Performance Using Artificial Neural Network. In Proceedings of the International Conference on High Voltage Engineering and Application, Shanghai, China, 17–20 September 2012; pp. 145–149.
41. Asimakopoulou, F.E.; Tsekouras, G.J.; Gonos, I.F.; Stathopoulos, I.A. Artificial Neural Network Approach on the Seasonal Variation of Soil Resistance. In Proceedings of the 7th Asia-Pacific International Conference on Lightning, Chengdu, China, 1–4 November 2011; pp. 794–799.
42. Johari, D.; Rahman, T.K.A.; Musirin, I. ANN Model Selection and Performance Evaluation for Lightning Prediction System. In Proceedings of the 2nd Seminar on Engineering and Information Technology, Kota Kinabalu, Sabah, Malaysia, 8–9 July 2009; pp. 321–325.
43. Salam, M.A.; Al-Alawi, S.M.; Maqrashi, A.A. An Artificial Neural Networks Approach to Model and Predict The Relationship Between The Grounding Resistance and Length of Buried Electrode in The Soil. *J. Electrostat.* **2006**, *64*, 338–342. [[CrossRef](#)]
44. Peterson, M.; Mach, D.; Buechler, D. A Global LIS/OTD Climatology of Lightning Flash Extent Density. *J. Geophys. Res. Atmos.* **2021**, *126*, e2020JD033885. [[CrossRef](#)]
45. Peterson, M.J.; Lang, T.J.; Bruning, E.C.; Albrecht, R.; Blakeslee, R.J.; Lyons, W.A.; Pédeboy, S.; Rison, W.; Zhang, Y.; Brunet, M.; et al. New World Meteorological Organization Certified Megaflash Lightning Extremes for Flash Distance (709 Km) and Duration (16.73 s) Recorded From Space. *Geophys. Res. Lett.* **2020**, *47*, e2020GL088888. [[CrossRef](#)]
46. Kucieńska, B.; Raga, G.B.; Manuel Torres-Puente, V. Climatology of Precipitation and Lightning Over the Pacific Coast of Southern Mexico Retrieved from Tropical Rainfall Measuring Mission Satellite Products and World Wide Lightning Location Network Data. *Int. J. Remote Sens.* **2012**, *33*, 2831–2850. [[CrossRef](#)]
47. Cahyo, R.H.D.; Ardimas; Anggara, Y.D.; Puspitasari, A. Peredianto Cloud to Ground Lightning Strike Density Analysis Based on Geographic Information System in Tuban Regency Area. *J. Phys. Conf. Ser.* **2023**, *2623*, 012006. [[CrossRef](#)]
48. Setiyawan, B.; Zakaria, A.; Wahono, E.P. Correlation Between the NASA's Tropical Rainfall Measuring Mission Data and Indonesia Meteorology and Geophysics Agency of Kalimantan Island. *Int. J. Aviat. Sci. Eng.* **2022**, *4*, 52–58.
49. Beiu, C.; Buica, G.; Antonov, A.E.; Risteiu, M. Photovoltaic System Protection Against Lightning. *MATEC Web Conf.* **2024**, *389*, 00070. [[CrossRef](#)]
50. Gagné, M.; Therriault, D. Lightning Strike Protection of Composites. *Prog. Aerosp. Sci.* **2014**, *64*, 1–16. [[CrossRef](#)]
51. Bouchard, A.; Buguet, M.; Chan-Hon-Tong, A.; Dezert, J.; Lalande, P. Comparison of Different Forecasting Tools for Short-Range Lightning Strike Risk Assessment. *Nat. Hazards* **2023**, *115*, 1011–1047. [[CrossRef](#)]
52. Adekitan, A.; Rock, M. Application of Machine Learning to Lightning Strike Probability Estimation. In Proceedings of the International Conference on Electrical Engineering and Informatics (ICELTICs), Aceh, Indonesia, 27–28 October 2020; pp. 1–9.
53. Maslowski, G.; Rakov, V.A.; Ziemba, R. Experimental Investigation and Modeling of Surge Currents in Lightning Protection System. In Proceedings of the 31th URSI General Assembly and Scientific Symposium (URSI GASS), Beijing, China 16–23 August 2014; pp. 1–4.
54. Sulik, S. Formation Factors of the Most Electrically Active Thunderstorm Days Over Poland (2002–2020). *Weather Clim. Extrem.* **2021**, *34*, 100386. [[CrossRef](#)]
55. Karmakar, S. Climatology of Thunderstorm Days Over Bangladesh During the Pre-Monsoon Season. *Bangladesh J. Sci. Tech.* **2001**, *3*, 103–122.
56. Pinto, O.; Pinto, I.R.C.A.; Ferro, M.A.S. A Study of the Long-Term Variability of Thunderstorm Days in Southeast Brazil. *J. Geophys. Res. Atmos.* **2013**, *118*, 5231–5246. [[CrossRef](#)]
57. Singh, O.; Bhardwaj, P. Spatial and Temporal Variations in the Frequency of Thunderstorm Days Over India. *Weather* **2019**, *74*, 138–144. [[CrossRef](#)]
58. Mannan, A.; Karmakar, S.; Devsarma, S.K. Climate Feature of the Thunderstorm Days and Thunderstorm Frequency in Bangladesh. In Proceedings of the Seminar on Application of Weather and Climate Forecasts in the Socio-economic Development and Disaster Mitigation, Dhaka, Bangladesh, 5–7 August 2008; pp. 11–27.

59. Czernecki, B.; Taszarek, M.; Kolendowicz, L.; Szyga-Pluta, K. Atmospheric Conditions of Thunderstorms in the European Part of the Arctic Derived from Sounding and Reanalysis Data. *Atmos. Res.* **2015**, *154*, 60–72. [CrossRef]
60. Popykina, A.; Ilin, N.; Shatalina, M.; Price, C.; Sarafanov, F.; Terentev, A.; Kurkin, A. Thunderstorms Near the North Pole. *Atmosphere* **2024**, *15*, 310. [CrossRef]
61. Mata, C.T.; Bonilla, T. Lightning Risk Assessment Tool, Implementation of the IEC 62305-2 Standard on Lightning Protection. In Proceedings of the 2012 International Conference on Lightning Protection (ICLP), Vienna, Austria, 2–7 September 2012; pp. 1–8.
62. IEC 62305-3; Protection against Lightning—Part 3: Physical Damage to Structures and Life Hazard. IEC Central Office: Geneva, Switzerland, 2010.
63. Lucietti, T.; Coelho, V.L.; Canever, G.D.L. Simulation of a Lightning Protection System Considering the Different Protection Levels. In Proceedings of the International Symposium on Lightning Protection (XV SIPDA), Sao Paulo, Brazil, 30 September–4 October 2019; pp. 1–8.
64. Amaral, F.C.L.; de Souza, A.N.; Zago, M.G. A Novel Approach To Model Grounding Systems Considering the Influence of High Frequencies. In Proceedings of the 5th Latin-American Congress on Electricity Generation & Transmission (CLAGTEE 2003), Sao Pedro, Brasil; 2003. Available online: https://www.researchgate.net/profile/Andre-Souza-15/publication/228731515_A_novel_approach_to_model_grounding_systems_considering_the_influence_of_high_frequencies/links/5593fd9908ae16f493efc617/A-novel-approach-to-model-grounding-systems-considering-the-influence-of-high-frequencies.pdf (accessed on 13 September 2024).
65. Parise, G.; Gatta, F.M.; Lauria, S. Common Grounding System. In Proceedings of the IEEE Systems Technical Conference on Industrial and Commercial Power, IEEE, Saragota Springs, NY, USA, 8–12 May 2005; pp. 184–190.
66. Androvitsaneas, V.P.; Gonos, I.F.; Stathopoulos, I.A. Research and Applications of Ground Enhancing Compounds in Grounding Systems. *IET Gener. Transm. Distrib.* **2017**, *11*, 3195–3201. [CrossRef]
67. Araujo, A.R.J.; Colqui, J.S.L.; Kurokawa, S.; Pissolato, J. A New Approach to Compute Grounding Impedance of Rods in a Frequency Dependent Multi-Layer Soil. In Proceedings of the IEEE Power & Energy Society General Meeting, Montreal, QC, Canada, 2–6 August 2020; pp. 1–5.
68. Androvitsaneas, V.P.; Gonos, I.F.; Stathopoulos, I.A. Artificial Neural Network Methodology for the Estimation of Ground Enhancing Compounds Resistance. *IET Sci. Meas. Technol.* **2014**, *8*, 552–570. [CrossRef]
69. Calixto, W.P.; Neto, L.M.; Wu, M.; Yamanaka, K.; da Paz Moreira, E. Parameters Estimation of a Horizontal Multilayer Soil Using Genetic Algorithm. *IEEE Trans. Power Deliv.* **2010**, *25*, 1250–1257. [CrossRef]
70. Mialdea-Flor, I.; Segura-Garcia, J.; Felici-Castell, S.; Garcia-Pineda, M.; Alcaraz-Calero, J.M.; Navarro-Camba, E. Development of a Low-Cost IoT System for Lightning Strike Detection and Location. *Electronics* **2019**, *8*, 1512. [CrossRef]
71. Neamt, L.; Chiver, O.; Barz, C.; Costea, C.; Erdei, Z. Considerations About Power System Grounding for Different Soil Structure. In Proceedings of the International Conference and Exposition on Electrical and Power Engineering (EPE), Iasi, Romania, 16–18 October 2014; pp. 1034–1038.
72. Voon, V.K.; Wong, K.I.; Tiong, T.C.; Mansour, A.; Law, K.H. Grounding Grid Design in Electrical Power Substation Using Optimization Methods. In Proceedings of the IOP Conference Series: Materials Science and Engineering, Sarawak, Malaysia, 26–28 November 2018; Volume 495, pp. 1–11.
73. Trifunovic, J.; Kostic, M. An Algorithm for Estimating the Grounding Resistance of Complex Grounding Systems Including Contact Resistance. *IEEE Trans. Ind. Appl.* **2015**, *51*, 5167–5174. [CrossRef]
74. Panagoulia, D.; Tsekouras, G.J.; Kousiouris, G. A Multi-Stage Methodology for Selecting Input Variables in ANN Forecasting of River Flows. *Glob. NEST J.* **2017**, *19*, 49–57. [CrossRef]
75. Leal, A.G.; López-Salamanca, H.L.; Lazzaretti, A.E.; Marcilio, D.C. A New Approach for Ground Resistance Measurements in Onshore Wind Farms Based on Clamp-On Meters and Artificial Neural Network. *Electr. Power Syst. Res.* **2022**, *210*, 108161. [CrossRef]
76. Collins, W.G.; Tissot, P. Thunderstorm Predictions Using Artificial Neural Networks. In *Artificial Neural Networks—Models and Applications*; Rosa, J.L.G., Ed.; InTech: Takasago, Japan, 2016; pp. 251–287.
77. Asimakopoulou, F.E.; Tsekouras, G.J.; Gonos, I.F.; Stathopoulos, I.A. Estimation of Seasonal Variation of Ground Resistance Using Artificial Neural Networks. *Electr. Power Syst. Res.* **2013**, *94*, 113–121. [CrossRef]
78. Asimakopoulou, F.E.; Kontargyri, V.T.; Tsekouras, G.J.; Gonos, I.F.; Stathopoulos, I.A. Estimation of the Earth Resistance by Artificial Neural Network Model. *IEEE Trans. Ind. Appl.* **2015**, *51*, 5149–5158. [CrossRef]
79. Alves, E.; Leal, A.; Lopes, M.; Fonseca, A. Performance Analysis Among Predictive Models of Lightning Occurrence Using Artificial Neural Networks and SMOTE. *IEEE Lat. Am. Trans.* **2021**, *19*, 755–762. [CrossRef]
80. Ekonomou, L.; Iracleous, D.P.; Gonos, I.F.; Stathopoulos, I.A. Lightning Performance Identification of High Voltage Transmission Lines Using Artificial Neural Networks. *Eng. Intell. Syst.* **2005**, *13*, 189–193.
81. Ullah, I.; Baharom, M.N.R.; Ahmad, H.; Wahid, F.; Luqman, H.M.; Zainal, Z.; Das, B. Smart Lightning Detection System for Smart-City Infrastructure Using Artificial Neural Network. *Wirel. Pers. Commun.* **2019**, *106*, 1743–1766. [CrossRef]
82. de Franco, R.; Biella, G.; Tosi, L.; Teatini, P.; Lozej, A.; Chiozzotto, B.; Giada, M.; Rizzetto, F.; Claude, C.; Mayer, A.; et al. Monitoring the Saltwater Intrusion by Time Lapse Electrical Resistivity Tomography: The Chioggia Test Site (Venice Lagoon, Italy). *J. Appl. Geophys.* **2009**, *69*, 117–130. [CrossRef]

83. Mi, X.; Zou, Y.; Wei, W.; Ma, K. Testing the Generalization of Artificial Neural Networks with Cross-Validation and Independent-Validation in Modelling Rice Tillering Dynamics. *Ecol. Modell.* **2005**, *181*, 493–508. [[CrossRef](#)]
84. Xu, Y.; Goodacre, R. On Splitting Training and Validation Set: A Comparative Study of Cross-Validation, Bootstrap and Systematic Sampling for Estimating the Generalization Performance of Supervised Learning. *J. Anal. Test.* **2018**, *2*, 249–262. [[CrossRef](#)] [[PubMed](#)]

Disclaimer/Publisher’s Note: The statements, opinions and data contained in all publications are solely those of the individual author(s) and contributor(s) and not of MDPI and/or the editor(s). MDPI and/or the editor(s) disclaim responsibility for any injury to people or property resulting from any ideas, methods, instructions or products referred to in the content.